Assessment of SeaWiFS Atmospheric and Marine Products for the Northern Adriatic Sea

Frédéric Mélin, Giuseppe Zibordi, and Jean-François Berthon

***Abstract*—An evaluation of the accuracy of atmospheric and marine satellite-derived products is presented and discussed for the northern Adriatic Sea coastal region using match-ups of *in situ* and Sea-Viewing Wide-Field-of-View Sensor (SeaWiFS) data for the period September 1997–September 2001. The study, making use of a simple atmospheric correction scheme including a near-infrared (NIR) turbid-water correction, has shown mean relative percentage differences between *in situ* and satellite-derived aerosol optical thickness lower than 23% in the spectral range between 443 and 865 nm. By applying regional empirical bio-optical algorithms for chlorophyll a concentration (*Chla*), total suspended matter concentration (TSM), and diffuse attenuation coefficient at 490 nm K_d(490), match-ups analysis has shown mean relative percentage differences of 40% for *Chla*, 28% for TSM, and 30% for K_d(490). The analysis is supported by comparison of *in situ* and satellite-derived normalized water leaving radiances nL_w to highlight the importance of the NIR turbid-water correction and to discuss the intrinsic uncertainties due to the use of empirical algorithms.**

***Index Terms*—Ocean color, remote sensing, SeaWiFS, validation.**

I. Introduction

THE SEA-VIEWING Wide-Field-of-View Sensor (SeaWiFS) [1], a visible and near-infrared (NIR) multispectral scanner, has been providing the scientific community with a global coverage of the ocean since 1997. End products derived from SeaWiFS imagery are extensively used for the study of marine phytoplankton biomass distribution and production (e.g., [2]–[5]), and of aerosol load (e.g., [6] and [7]). The relevance and the wide range of applications underline the need of a continuous and extensive effort in assessing and improving the accuracy of the derived products [8].

To fully support the former objective, high-accuracy *in situ* measurements are essential for both the vicarious calibration of the space sensor and the validation of the derived products, and have been considered a major objective of the SeaWiFS project [9].

A processing tool has been developed for the analysis of SeaWiFS imagery, making use of vicarious calibration to minimize uncertainties in absolute sensor calibration and radiative transfer modeling of the atmospheric processes. This study aims at assessing the accuracy of SeaWiFS-derived products like aerosol optical thickness, chlorophyll a, total suspended matter and diffuse attenuation coefficient routinely generated for the Adriatic Sea, using an extensive time series of atmospheric and marine measurements performed at a coastal site.

Manuscript received May 14, 2002; revised November 8, 2002. This work was supported through the COAST and GEIS JRC institutional projects and in part by the European Commission under Contract MAS3CT970087 (COLORS project).

F. Mélin and G. Zibordi are with the Inland and Marine Waters Unit, Joint Research Centre, 21020 Ispra (VA), Italy (e-mail: frederic.melin@jrc.it; giuseppe.zibordi@jrc.it).

J.-F. Berthon was with the Inland and Marine Waters Unit, Joint Research Centre, 21020 Ispra (VA), Italy. He is now with the Maison de la Recherche en Environnement Naturel (MREN), Université du Littoral Côte d'Opale, 62930, Wimereux, France (e-mail: berthon@mren2.univ-littoral.fr).

Digital Object Identifier 10.1109/TGRS.2003.809939

II. *In Situ* Measurements

Field data for ocean color vicarious calibration and validation activities have been collected in the framework of the Coastal Atmosphere and Sea Time-Series (CoASTS) project at the Acqua Alta Oceanographic Tower (AAOT) (latitude 45°19′ N, longitude 12°30′ E) in the northern Adriatic Sea [10]. The measurement site is characterized by dominant continental aerosol and by seawater classified as Case 2 for a third of the measurement stations [11] according to a Case 1/Case 2 separation scheme suggested by Loisel and Morel [12].

A. Measurements Description

Optical measurements relevant to this work are 1) direct solar irradiance $E_s(\lambda)$ data from a CE-318 automatic sun-photometer for the computation of the aerosol optical thickness $\tau_a(\lambda)$ at 440, 500, 670, and 870 nm and 2) underwater optical profile data of upwelling radiance $L_u(z, \lambda)$, downward irradiance $E_d(z, \lambda)$, and upward irradiance $E_u(z, \lambda)$ from the Wire-Stabilized Profiling Environmental Radiometer (WISPER) system [13] for the computation of the normalized water leaving radiance $\mathrm{nL}_w(\lambda)$ [14] at nominal center wavelengths corresponding to SeaWiFS visible channels (412, 443, 490, 510, 555, and 670 nm).

The calibrated sun-photometer data $E_s(\lambda)$, assuming no gaseous absorption, are related to the atmospheric optical thickness $\tau(\lambda)$ through the Beer–Lambert–Bouguer law $E_s(\lambda) = E_0(\lambda)D^2 \exp(-\tau(\lambda)m)$, where $E_0(\lambda)$ is the extra-atmospheric mean solar irradiance; D^2 accounts for the sun-earth distance; m is the optical air mass; and $\tau(\lambda) = \tau_r(\lambda) + \tau_o(\lambda) + \tau_a(\lambda)$, i.e., the sum of the Rayleigh, ozone and aerosol optical thicknesses [15].

The normalized water leaving radiance $\mathrm{nL}_w(\lambda)$ at center-wavelength λ is computed according to

$$\mathrm{nL}_w(\lambda) = \frac{L_u(0^-, \lambda) \cdot t_{ss}(\lambda) \cdot E_0(\lambda).(1 - \rho_s(\lambda))}{[E_d(0^-, \lambda) - 0.49 \cdot E_u(0^-, \lambda)]} \quad (1)$$

where $L_u(0^-, \lambda)$, $E_d(0^-, \lambda)$, and $E_u(0^-, \lambda)$ are the subsurface upwelling radiance, downward irradiance, and upward irradiance, respectively, obtained from the least squares regression fit of the natural logarithm of profile radiance (i.e., $L_u(z, \lambda)$) and

irradiance (i.e., $E_d(z, \lambda)$ and $E_u(z, \lambda)$), corrected for instrument self-shading [16], [17], and tower shading effects [18]. The extra-atmospheric mean solar irradiance $E_0(\lambda)$ is taken from [19]; $t_{ss}(\lambda)$ is the sea surface transmittance from below to above water for upward radiance; and $\rho_s(\lambda)$ is the sea surface spectral reflectance for above water downward irradiance given by

$$\rho_s(\lambda) = \frac{\rho(\theta) + 0.066r(\lambda)}{1 + r(\lambda)} \tag{2}$$

where $\rho(\theta)$ is the Fresnel reflectance of the sea surface; the constant 0.066 is the sea surface albedo under diffuse illumination; and $r(\lambda)$ is the diffuse to direct solar irradiance ratio.

The optical *in situ* measurements are complemented by laboratory analysis of surface water samples for the determination of concentrations of total chlorophyll a (*Chla*) and total suspended matter (TSM) through High Performance Liquid Chromatography [20] and dry weighting techniques [21], respectively.

B. Measurement Uncertainties

The uncertainties related to the *in situ* measurements described above are briefly discussed with the aim of providing sensitivity to the comparison of *in situ* and satellite-derived products.

The uncertainty in the aerosol optical thickness $\tau_a(\lambda)$, assuming a proper calibration of the CE-318 sun-photometer, is estimated to be less than 0.02 [22].

The uncertainty associated with $\mathrm{nL}_w(\lambda)$ derived from *in situ* radiometric data has been estimated, taking into account the results presented in [10], [18], [23], and [24]. Assuming $E_u(0^-, \lambda) \ll E_d(0^-, \lambda)$, calculations have been carried out with a typical 1.5% uncertainty due to absolute radiometric calibration, 1.5% due to the immersion coefficients uncertainty, a maximum 2% uncertainty due to self-shading and tower-shading corrections, and a typical 3% uncertainty due to environmental perturbations (surface roughness, changes in seawater characteristics and illumination conditions during in-water profiling). An additional source of uncertainty in direct comparison of satellite and *in situ* $\mathrm{nL}_w(\lambda)$ is the value of $E_0(\lambda)$, which could be affected by differences in center-wavelength or bandwidth. This source of uncertainty has here been assumed to be lower than 3%. All the former uncertainties associated with the calculation of $\mathrm{nL}_w(\lambda)$, and assumed independent, give a quadratic sum of $\sim$5%, therefore matching the target selected for SeaWiFS calibration and validation activities [25], [8].

The uncertainty for *in situ Chla* is on average $\sim$7%, when the contribution of divinyl-chlorophyll a to total chlorophyll a is negligible [26]. An additional term (on average $\sim$6%) should be included in the uncertainty budget because of the nonhomogeneity of the sampled water volume in the considered coastal environment [10]. The quadratic sum of the two uncertainties for *Chla* leads to $\sim$10% total uncertainty. The uncertainty in measurements of TSM, simply estimated by the reproducibility of measurements from replicated samples, has shown average values of $\sim$14% [10].

C. Validation Dataset

The dataset for validation activities, including measurements between September 1997 and September 2001, contains 35 valid match-ups (i.e., coincident *in situ* and satellite data) for in-water and atmospheric data resulting from monthly CoASTS measurements campaigns, and 197 match-ups for direct solar irradiance, resulting from continuous operations of the autonomous CE-318 sun-photometer included in the Aerosol Robotic Network [15]. The former match-ups are used for the SeaWiFS vicarious calibration and the validation of marine products, whereas the latter are only applied for the validation of atmospheric products.

III. Satellite Products

The following section presents the elements required for satellite products development by introducing calibration, atmospheric correction, in-water algorithms, and satellite data.

A. Calibration

The calibration of SeaWiFS raw data into geophysical units is performed by removing the dark value (i.e., zero radiance), and applying a lookup table with the absolute prelaunch calibration factors [27]. A time-dependent correction, derived from lunar observations [28], is then utilized to compensate for the change of response with time for the various channels.

The uncertainties in the prelaunch calibration and in the modeling of the atmospheric radiative transfer processes are reduced by applying vicarious adjustment factors $V_{cf}(\lambda)$ [29], [30]. These factors are determined by minimizing the difference between *in situ* and satellite-derived normalized water leaving radiance for a set of selected coincident measurements. For the visible domain, $V_{cf}(\lambda)$ have been computed according to Sturm and Zibordi [31] with (3) (shown at the bottom of the next page). $\mathrm{nL}_w(\lambda)_{\mathrm{meas}}$ are the normalized water leaving radiance measured *in situ*. $\mathrm{nL}_w(\lambda)$ have been calculated from SeaWiFS calibrated data, processed with the atmospheric correction scheme given by Sturm and Zibordi [31] and subsequently corrected for spectral bandpass effects [32]. $L_r(\lambda)$ and $L_a(\lambda)$ are the Rayleigh and aerosol path radiances. $C_{\mathrm{ra}}(\lambda)$ is a correction factor accounting for Rayleigh–aerosol interactions. t_d is the atmospheric diffuse transmittance calculated as a function of wavelength and cosine of the zenith angle for the satellite sensor (μ) and the sun (μ_0). The calibration coefficient at 765 nm has been adjusted by a factor 0.953 in order to match the value of the Ångström exponent retrieved from aerosol optical thickness ground measurements for the same selected days, whereas the calibration coefficient at 865 nm is maintained at its prelaunch value. The last assumption is *a posteriori* justified by the relatively accurate retrieval of the aerosol optical thickness at 865 nm in the atmospheric correction process. A similar approach is described in [30].

It is stressed that the sensor plus the atmospheric correction scheme need to be viewed as a single system and calibrated accordingly [29]. Consequently, the vicarious calibration coefficients depend on the adopted atmospheric model. This explains the differences between the vicarious calibration coefficients applied here and those used in the SeaWiFS Data Analysis System (SeaDAS) [33] (version 4.3). These differences vary from 0.3% to 1% in the 443–765 nm interval and reach 1.5% at 412 nm.

B. Atmospheric Correction

Calibrated top-of-atmosphere SeaWiFS radiances are used to compute the radiance exiting the surface of the water by removing the atmospheric contribution from the total signal. The atmospheric correction algorithm is presented in [31], and it is only briefly outlined for completeness.

The atmospheric contribution for the bands at 765 and 865 nm is used to compute the aerosol radiance and optical thickness, and its value is extrapolated to shorter wavelengths. The model accounts for Rayleigh multiple scattering (scattering by atmospheric gas molecules), aerosol single scattering, and Rayleigh-aerosol coupling through an iterative process. With respect to the reference paper, Rayleigh radiance lookup tables have here been taken from SeaDAS version 4 [33], [34].

The turbid-water correction proposed by Arnone *et al.* [35] and implemented in [31] to account for the water leaving radiance contribution at 765 and 865 nm has also been modified. The normalized water leaving radiance can be linked to $R(\lambda)/Q(\lambda)$ [14] where $R(\lambda)$ is the ratio of subsurface upward to downward irradiance $E_u(0^-, \lambda)/E_d(0^-, \lambda)$, and $Q(\lambda)$ is the ratio of subsurface upward irradiance to upwelling radiance $E_u(0^-, \lambda)/L_u(0^-, \lambda)$.

The equation

$$\frac{R(\lambda)}{Q(\lambda)} = l_1 \left(\frac{b_b(\lambda)}{b_b(\lambda) + a(\lambda)} \right) + l_2 \left(\frac{b_b(\lambda)}{b_b(\lambda) + a(\lambda)} \right)^2 \quad (4)$$

with l_1 and l_2 equal to 0.0949 and 0.0794 [36] is solved at 670 nm to yield the ratio $b_b(\lambda)/(b_b(\lambda) + a(\lambda))$ with $b_b(\lambda)$ and $a(\lambda)$ total backscattering and absorption coefficients, respectively. The absorption coefficient is computed as the sum of the absorption by pure seawater and absorption by phytoplankton expressed as a function of the *Chla* according to [37]. Indeed, at 670 nm, the phytoplankton absorption may not be negligible with respect to pure seawater absorption, especially for high pigment concentrations. The total backscattering coefficient $b_b(\lambda)$ at 670 nm is then calculated, and its particulate component is obtained by subtracting the pure seawater value. The value of $b_b(\lambda)$ for particulate matter is here assumed constant in the spectral interval 670–865 nm. The calculation of the water leaving radiance in the channels at 765 and 865 nm is finally done through (4) and (1). For these NIR channels, the total absorption is that of pure seawater. The absorption coefficients for pure seawater are from [38] at 670 and 765 nm and [39] at 865 nm. The backscattering coefficients for pure seawater are computed from [40].

The correction process develops through nested iterations. At the first iteration, the water leaving radiance is assumed null at 765 and 865 nm to compute the aerosol radiance and the normalized water leaving radiance at all wavelengths. If the resulting water leaving radiance at 670 nm (i.e., calculated as the difference between the total radiance at the sensor and the atmospheric contribution) is negative, the scheme described above is not applicable. The inconsistency is overcome as proposed in [41] by using the chlorophyll a concentration resulting from a band ratio algorithm (see below) to directly estimate the value of the backscattering coefficient with an empirical parameterization developed for Case 1 waters [12], [42]. This solution only relies on valid (i.e., positive) values of the water leaving radiance at 555 nm and below. Nevertheless, using the water leaving radiance at 670 nm to derive the radiances at longer wavelengths is preferred when possible, because the resulting spectrum is constrained to be consistent. Moreover, the use of parameterizations developed for Case 1 waters to link *Chla* and backscattering is questionable for turbid waters, as already stated by Siegel *et al.* [41]. Alike is the assumption of absorption only due to phytoplankton at 670 nm in turbid waters. However, the numerical weight of the latter assumption is secondary in the proposed correction process for the considered geographic area.

The outputs of the atmospheric correction algorithm include the aerosol radiance and optical thickness at all channels, and the normalized water leaving radiance at the first six channels. The latter is used to compute the concentrations of optically significant constituents.

C. Empirical Algorithms for Seawater Constituents

Empirical algorithms for the retrieval of surface *Chla* and TSM concentrations were developed by Berthon *et al.* [11] using the CoASTS *in situ* dataset collected between 1995 and 1998. They make use of ratios of the underwater remote sensing reflectance $R_{\rm rs}(\lambda) = L_u(0^-, \lambda)/E_d(0^-, \lambda)$. These algorithms are hereafter referred to as AD (standing for Adriatic).

The AD *Chla* algorithm, similarly to the open ocean SeaWiFS OC2v4 polynomial algorithm [43], combines the two 490- and 555-nm bands. The adopted relationship is (expressed in milligrams per cubic meter)

$$\text{Chla} = 10^{0.091 - 2.620 R_{35} - 1.148 R_{35}^2 - 4.949 R_{35}^3} \quad (5)$$

where R_{35} is $\log_{10}[R_{\rm rs}(490\ \text{nm})/R_{\rm rs}(555\ \text{nm})]$. Equation (5) was developed with $n = 109$ points, and exhibits a determination coefficient $r^2 = 0.77$ and an rms of relative difference (RMSRD) of 42%. The *Chla* algorithm yields much lower values than OC2v4 in the range 0.1–1.0 mg m^{-3}, whereas the two algorithms tend to converge for higher concentrations.

A similar algorithm was developed for the retrieval of TSM (expressed in grams per cubic meter)

$$\text{TSM} = 10^{0.967 - 1.169 R_{46}} \quad (6)$$

where R_{46} is $\log_{10}[R_{\rm rs}(510\ \text{nm})/R_{\rm rs}(670\ \text{nm})]$, with $n = 109$ samples, determination coefficient $r^2 = 0.66$, and RMSRD = 39%.

These relationships for *Chla* and TSM were validated on the CoASTS data collected in 1999 and 2000. The comparison

$$V_{cf}(\lambda) = \frac{C_{\rm ra}(\lambda) \cdot [L_a(\lambda) + L_r(\lambda)] + t_d(\lambda, \mu) \cdot t_d(\lambda, \mu_0) \cdot \text{nL}_w(\lambda)_{\rm meas} \cdot \mu_0 \cdot D^2}{C_{\rm ra}(\lambda) \cdot [L_a(\lambda) + L_r(\lambda)] + t_d(\lambda, \mu) \cdot t_d(\lambda, \mu_0) \cdot \text{nL}_w(\lambda) \cdot \mu_0 \cdot D^2} \quad (3)$$

between modeled and measured concentrations showed an RMSRD of 43.1% and 36.4%, respectively, well in keeping with the RMSRD associated with the algorithms and providing an estimate of their intrinsic uncertainties.

Analogously to the algorithm proposed by Mueller [44], and adopted for the third reprocessing of SeaWiFS data by the National Aeronautics and Space Administration [45], a relationship has been proposed by Berthon *et al.* [11] for the retrieval of the diffuse attenuation coefficient at 490 nm, $K_d(490)$, for an optically homogeneous surface layer (expressed in units per meter)

$$K_d(490) = 0.016 + 0.205.[L_{35}]^{-1.754} \tag{7}$$

where L_{35} is $\mathrm{nL}_w(490\ \mathrm{nm})/\mathrm{nL}_w(555\ \mathrm{nm})$, with $n = 109$ samples, $r^2 = 0.80$, and RMSRD $= 23\%$. A validation of the algorithm carried out with data from 1999 and 2000 shows an RMSRD of 44.1%.

The offset 0.016 m^{-1} in (7) is the constant value of $K_d(490)$ for "pure" seawater adopted in [44]. Compared to Mueller [44], the present algorithm has a higher exponent (i.e., -1.754 versus -1.5401) and thus yields higher values of $K_d(490)$ for the range 0.2–0.5 m^{-1} (a range not represented in the development dataset considered in [44]).

D. Satellite Data

All the SeaWiFS imagery of the northern Adriatic area for the study period (September 1997–September 2001) has been collected and archived. The SeaWiFS dataset includes full-resolution local area coverage images regularly recorded onboard the satellite or obtained from various European receiving stations and amounts to 1925 scenes. Images corresponding to days of measurements on the platform have been processed with the algorithms previously described. For each scene, the pixel closest to the location of the AAOT is searched, and the code outputs are saved for a 3×3 pixel square centered on that pixel.

IV. Products Validation

This section presents the comparison of satellite-derived and *in situ* measured quantities, namely the aerosol optical thickness τ_a, the normalized water leaving radiance nL_w, the diffuse attenuation coefficient at 490 nm K_d, the near-surface concentrations of chlorophyll a *Chla*, and total suspended matter TSM. For the comparison, the days for which a given quantity is available from both sources are individuated, and the related pairs of satellite-derived and *in situ* data are referred to as match-ups. When several *in situ* measurements or two satellite passes are available for a given day, the most coincident pairs are selected. Scenes where the site is observed with a high satellite zenith angle (higher than 56°) are discarded. Indeed, high satellite zenith angles increase the atmospheric path length, leading to a possible degradation of the performance of the atmospheric correction scheme. In addition, high viewing angles correspond to pixels characterized by reduced spatial resolution that lessens the significance of the comparison with *in situ* data from a point site. The other exclusion criteria (flags) are the presence of a cloud, the detection of sun glint conditions, a sun zenith angle higher than 70°, or a failure of the atmospheric correction.

A. Atmospheric Products

The analysis of *in situ* and remote sensing aerosol values has given 197 match-ups. It is emphasized that the measurement site, a small tower located eight nautical miles from the shore, is ideal for comparison exercises because the structure holding the instruments and the nearby coastal land do not significantly perturb the radiation field viewed by the space sensor around the site.

A match-up was considered valid if, for all elements of a 3×3 pixel square centered on the measurement site (i.e., the AAOT), the atmospheric correction was successful (no flagging according to the exclusion criteria listed above) and resulted in a retrieval of aerosol optical thickness in all eight channels and positive water leaving radiance in the first five channels. In addition, match-ups for which a high variability around the site was detected were discarded too. Following Bailey and Wang [46], match-ups were ignored if the ratio of the standard deviation to the mean value of the aerosol optical thickness at 865 nm computed over the 3×3 pixel square, was greater than 0.2. For each match-up, the *in situ* value was computed as the average of measurements taken over a 2–h time slot (± 1 h from the satellite pass). Moreover, conditions of high temporal variability were filtered out in a similar way as for remote sensing data: the match-up was not considered valid if the standard deviation of the *in situ* measurements normalized by their average was greater than 0.2 or if only one measurement was recorded during the time slot.

Fig. 1 displays the comparison for channels centered at 443, 500, 670, and 865 nm (the aerosol optical thickness at 500 nm measured from the ground is compared with a simple average of the satellite values at 490 and 510 nm). The agreement between measured and satellite-derived aerosol optical thickness shows a determination coefficient r^2 higher than 0.81, a mean relative percentage difference d (defined as the average ratio of the absolute difference of remotely sensed and *in situ* values divided by the *in situ* value, and expressed as percentage) between 17% and 23% for the different channels. Remote sensing values show a slight underestimate of the aerosol optical thickness at 500 and 670 nm, especially for low aerosol loads.

The Ångström [47] exponent is computed by linear regression, as a function of wavelength, of the log-transformed aerosol optical thickness between 440 and 870 nm and between 443 and 865 nm for *in situ* and remote sensing data, respectively. Fig. 2 shows comparison between satellite-derived and *in situ* values of the Ångström exponent. Results exhibit an underestimate of the satellite-derived with respect to *in situ* data, with averages of 1.66 and 1.76 and standard deviations of 0.23 and 0.29, respectively. The atmosphere at the site appears dominated by aerosols from continental origin with Ångström exponent values actually close to those recorded at an inland measurement site (i.e., Ispra site, 500 km further west of the AAOT site, in the Po valley [48]).

If the restriction on the time difference between ground and satellite measurements is relaxed to ± 4 h, some extra match-ups compare quite badly with *in situ* values. Conversely, the statistics are not significantly affected if the viewing angle limit is extended up to 67°. Thus, the results appear fairly robust with

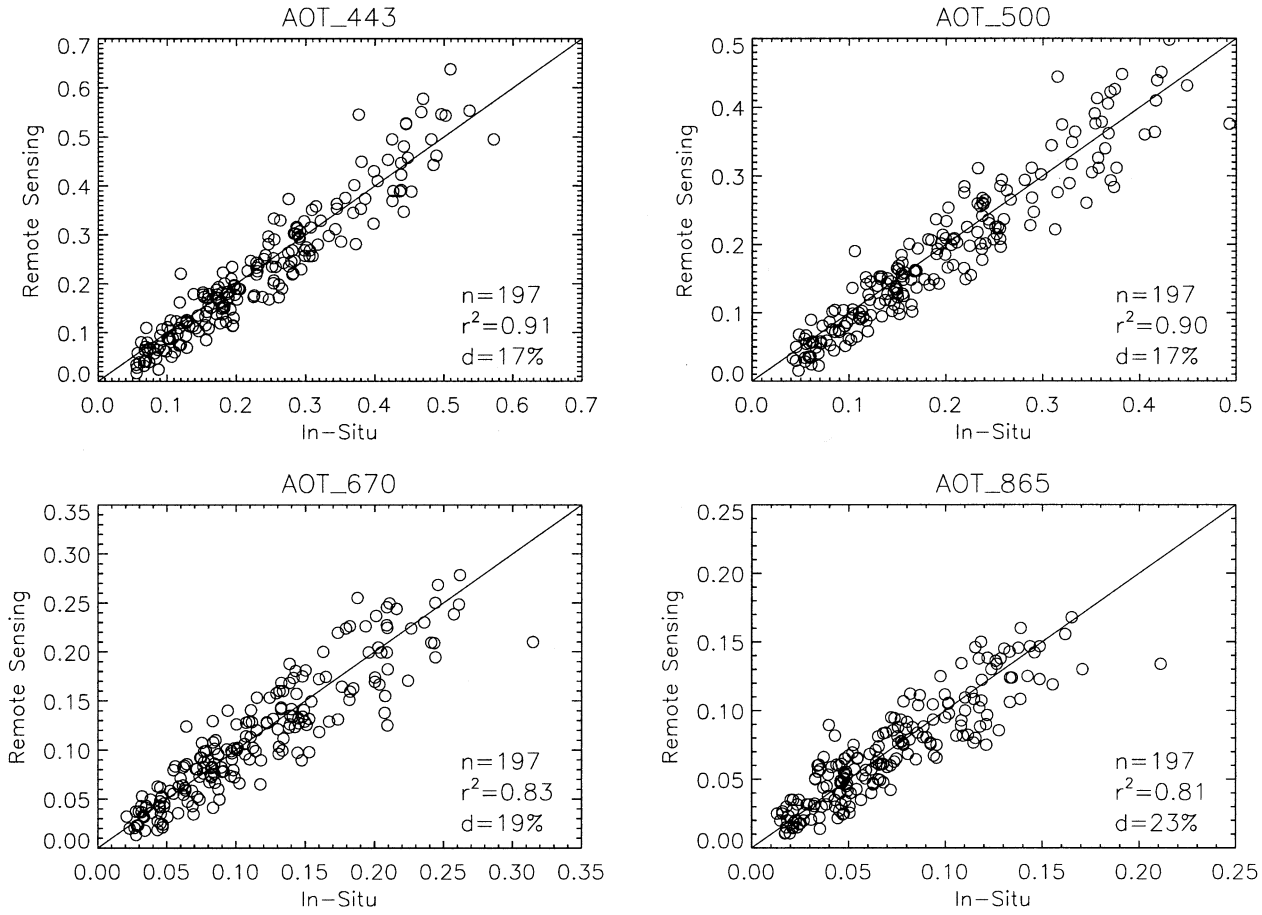

Fig. 1. Scatter plot of SeaWiFS-derived versus *in situ* aerosol optical thickness at 443, 500, 670, and 865 nm. n is the number of match-ups; r^2 is the coefficient of determination; and d is the mean relative percentage difference between the two datasets.

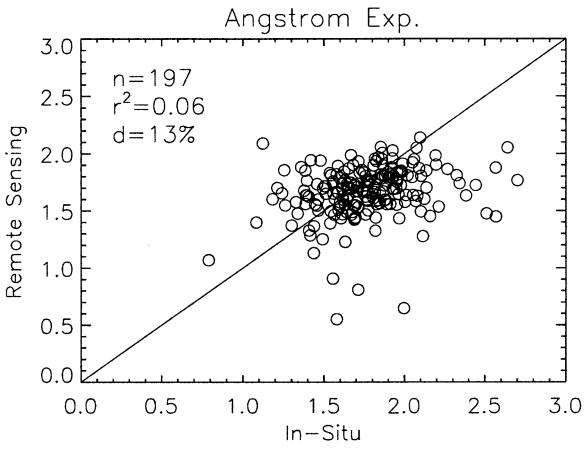

Fig. 2. Scatter plot of SeaWiFS-derived versus *in situ* Ångström exponents for the match-ups shown in Fig. 1.

respect to the conditions of observation but are more sensitive to the possible changes in the atmospheric conditions that may occur as a function of time between *in situ* measurements and satellite overpass.

B. Marine Optical Properties

The number of match-ups, for the validation of marine products, is limited to 35. Three match-ups with optimal conditions were used for the calculation of the vicarious calibration coefficients following the scheme given in [31]. Match-ups for the marine optical properties include a valid remote sensing retrieval (no flagging according to the criteria listed above) for all 3×3 pixels surrounding the platform and positive water leaving radiance in all first six channels (i.e., only data with entire spectra are retained for the analysis). Except for five match-ups, all *in situ* measurements were performed within 1 h of the satellite overpass.

Fig. 3 shows the comparison between observed and remotely sensed normalized water leaving radiance for the different channels from 412–670 nm. The determination coefficient is greater than 0.79 for the channels above 443 nm but decreases for the blue part of the spectrum. The mean relative percentage difference d is less than 20% for the channels at 490, 510, and 555 nm, but as high as 47% and 30% at 412 and 443 nm, respectively.

At 670 nm, the mean relative percentage difference d is 29%, with four satellite retrievals characterized by a very low normalized water leaving radiance (below 0.02 mW $cm^{-2}sr^{-1}\mu m^{-1}$). To highlight the relevance of the turbid-water correction, Fig. 4 displays a scatter plot of the normalized water leaving radiance at the representative wavelengths 412, 555, and 670 nm, calculated using the atmospheric correction scheme with and without the turbid-water correction. In the latter case, the number of match-ups is decreased to 31 because cases with at least one pixel characterized by a negative water leaving radiance at

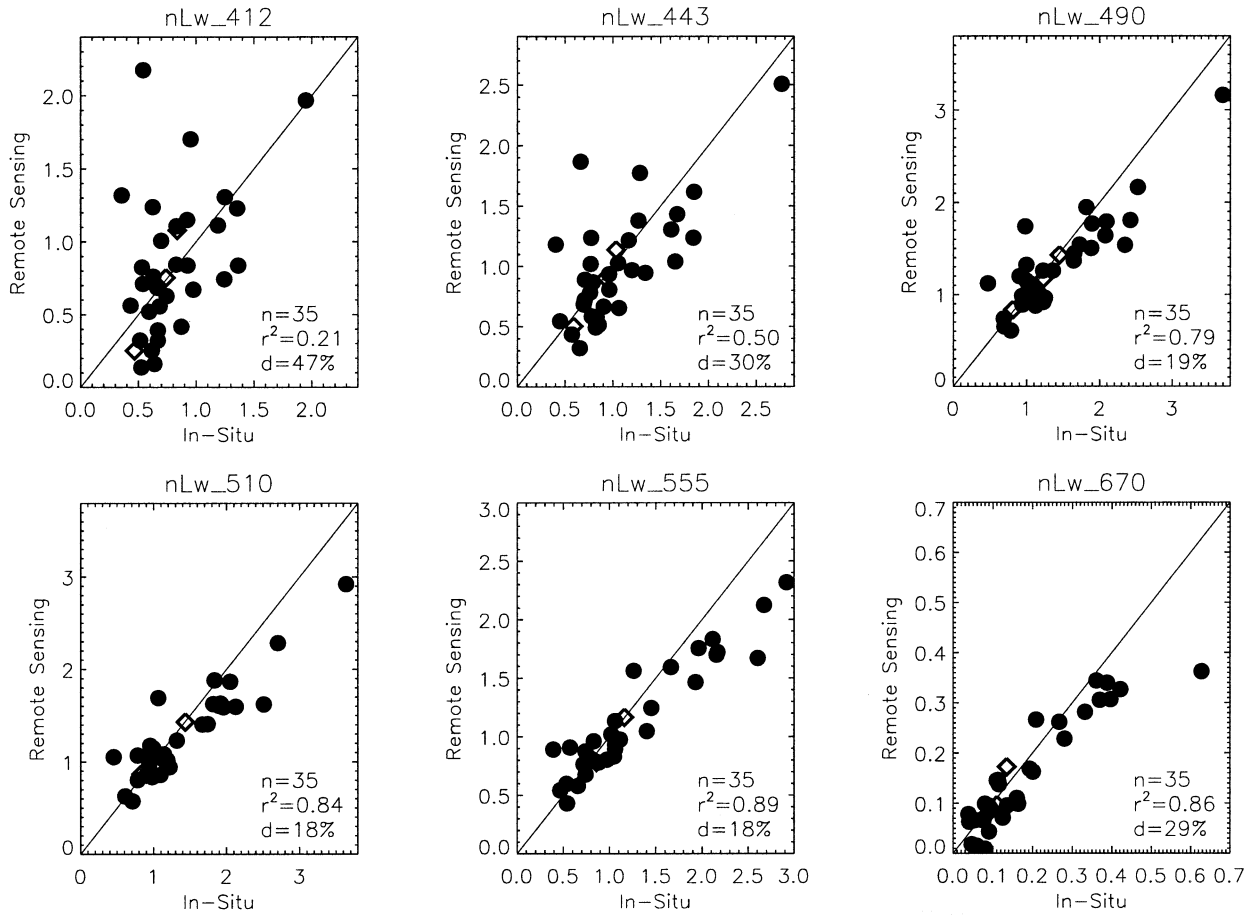

Fig. 3. Scatter plot of SeaWiFS-derived versus *in situ* normalized water leaving radiance nL_w from 412–670 nm. The remote sensing values are the average over a 3×3 pixel square. Match-ups include a valid remote sensing retrieval for all 3×3 pixels surrounding the platform and positive water leaving radiance in all the first six channels. In addition, the satellite zenith angle is restricted to 56°. The diamond symbols represent the match-ups used for the determination of the vicarious calibration coefficients.

670 nm are discarded. At all wavelengths, the normalized water leaving radiance without correction is systematically below the value obtained with correction. For these 31 match-ups, the mean relative percentage difference d between remotely sensed and *in situ* normalized water leaving radiance at 670 nm is equal to 25% if the turbid-water correction is applied, and to 36% if it is not. The turbid-water correction results in an average increase of 29% for the radiance at 670 nm (Fig. 4). The impact of the correction is weaker for the central channels but is again significant for the blue band at 412 nm, improving the comparison with *in situ* measurements. For the 31 match-ups considered, the values of r^2 and d between remotely sensed and *in situ* normalized water leaving radiance at 412 nm are equal to 0.18 and 45% with correction, and to 0.12 and 49% without correction. These improvements are of the same order of magnitude as those obtained in [41].

The relative difference between remote sensing and *in situ* measurements has been analyzed as a function of the angles of illumination and observation, the time difference between the two measurements, and the spatial variability within the 3×3 pixel matrix centered on the measurement point. No clear relationship has been found with respect to the geometry or time of observation, even though, on average, the relative difference between remote sensing and *in situ* data tends to be higher for cases where the site was viewed with a high observation angle (i.e., up to 67°) or with a significant time difference (i.e., up to 4 h). A similar conclusion is drawn for match-ups that are characterized by a high variability around the measurement site (i.e., a standard deviation of nL_w at 555 nm divided by the mean value, higher than 0.2). It is worth reminding that the spatial nature of the quantities compared in the analysis is very different. The *in situ* measurements are representative of a small area, whereas the signal at the space sensor is integrated over the field of view. The size of the sensor footprint is 1.1 km at nadir and increases with the observation angle, reaching a 2-km length with an observation angle of ∼43°. So, a high satellite viewing angle is a factor diminishing the significance of the comparison with observed quantities at a single point. Likewise, a high spatial variability is an indicator of local heterogeneity that limits the value of the comparison.

If the analysis is restricted to satellite data with pixels not larger than 2 km (i.e., observed with a viewing angle smaller than 43°), and also a standard deviation normalized to the mean value smaller than 0.2 (calculated for the water leaving radiance at 555 nm), the statistics are significantly improved for the 22 match-ups left. As shown in Fig. 5, the mean relative percentage difference d is below 13% for the wavelengths 490–555 nm, and the determination coefficient is above 0.92. The improvement is

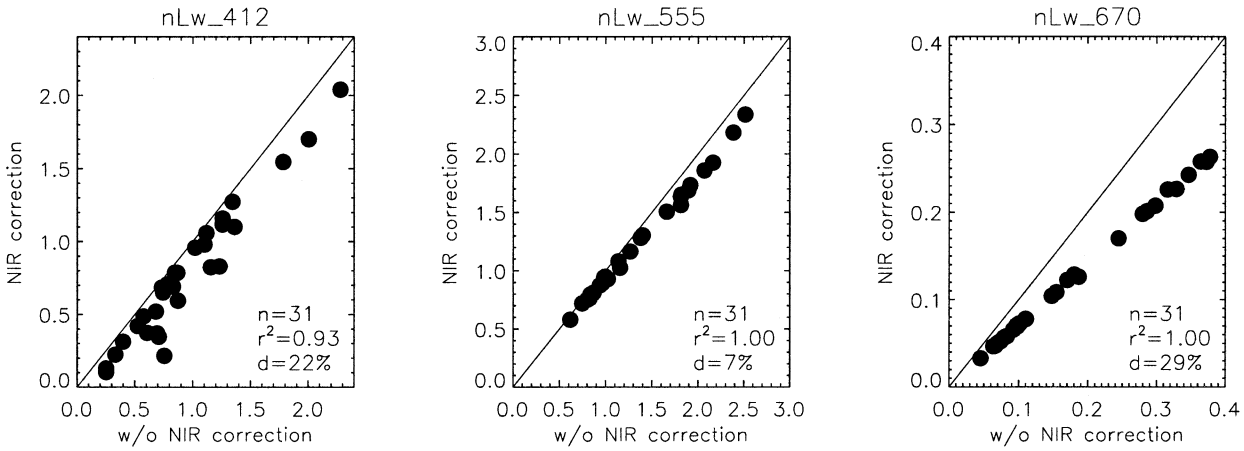

Fig. 4. Scatter plot of SeaWiFS-derived normalized water leaving radiance nL_w at 412, 555, and 670 nm, without versus with turbid-water (NIR) correction.

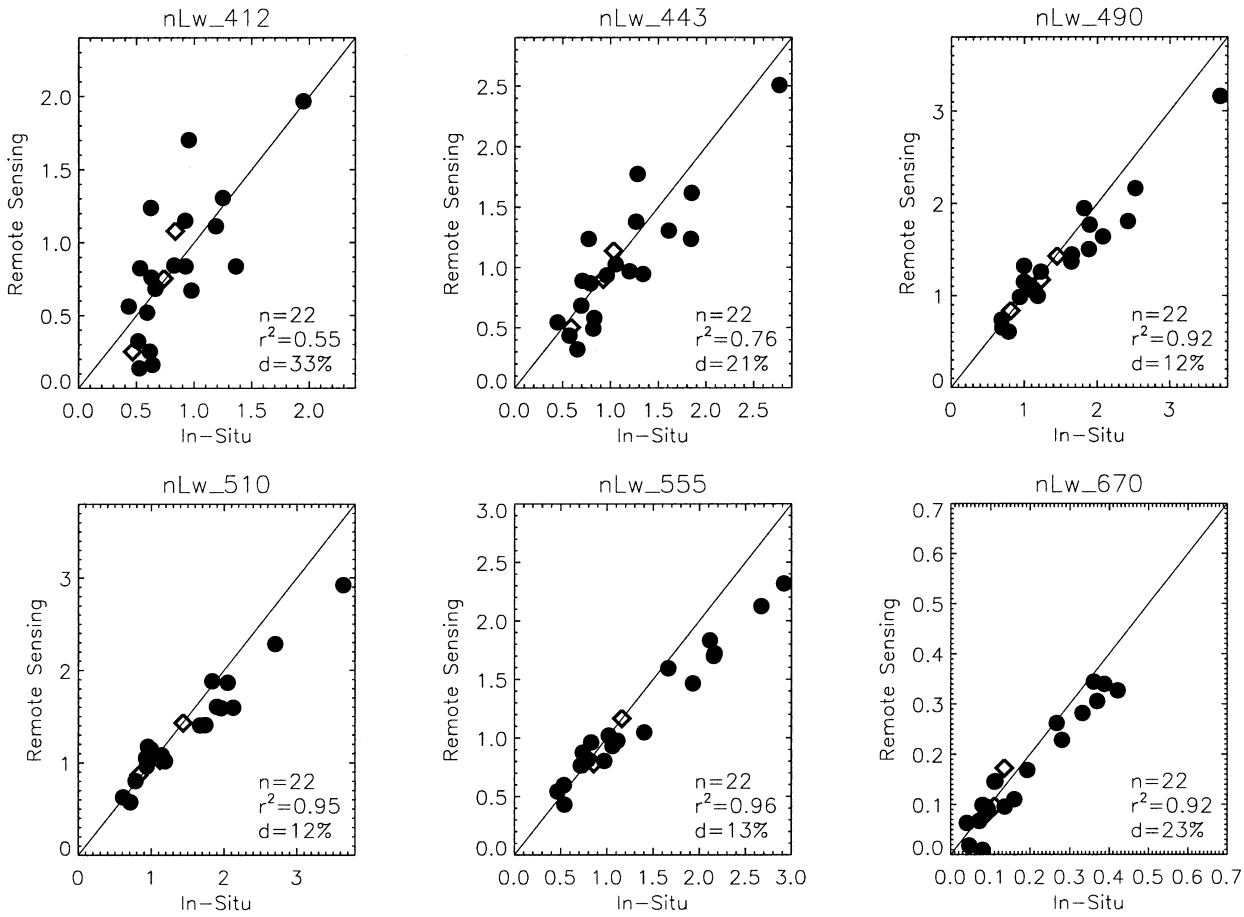

Fig. 5. Scatter plot of SeaWiFS-derived versus *in situ* normalized water leaving radiance nL_w from 412–670 nm. Match-ups are restricted to viewing angles lower than 43° and to a ratio lower than 0.2 for the standard deviation divided by the mean value, calculated for the normalized water leaving radiance at 555 nm over the 3 × 3 pixel square around the measurement site. The diamond symbols represent the match-ups used for the determination of the vicarious calibration coefficients.

as well significant for the blue part of the spectrum with relative mean percentage differences d of 33% and 21% at 412 and 443 nm, respectively.

The ratios of $R_{\rm rs}$ or nL_w in channels 3 and 5 (490 and 555 nm), and 2 and 5 (443 and 555 nm) are often used in empirical algorithms for the calculation of *Chla* (see [49] and references therein, [43], and [50]) or for the calculation of K_d [44], [51]. Fig. 6 exhibits a close agreement between measured and satellite-derived ratios $nL_w(490\ \text{nm})/nL_w(555\ \text{nm})$, with a mean relative difference of 8%. The agreement for the ratio $nL_w(443\ \text{nm})/nL_w(555\ \text{nm})$ is degraded (i.e., showing $d = 20\%$), because of the larger differences observed at 443 nm between satellite and *in situ* data. The ratio of the normalized water leaving radiance at 510 and 670 nm also displays a slight overestimate with a mean relative percentage difference d of 20% [the ratio of the reflectance at these two wavelengths

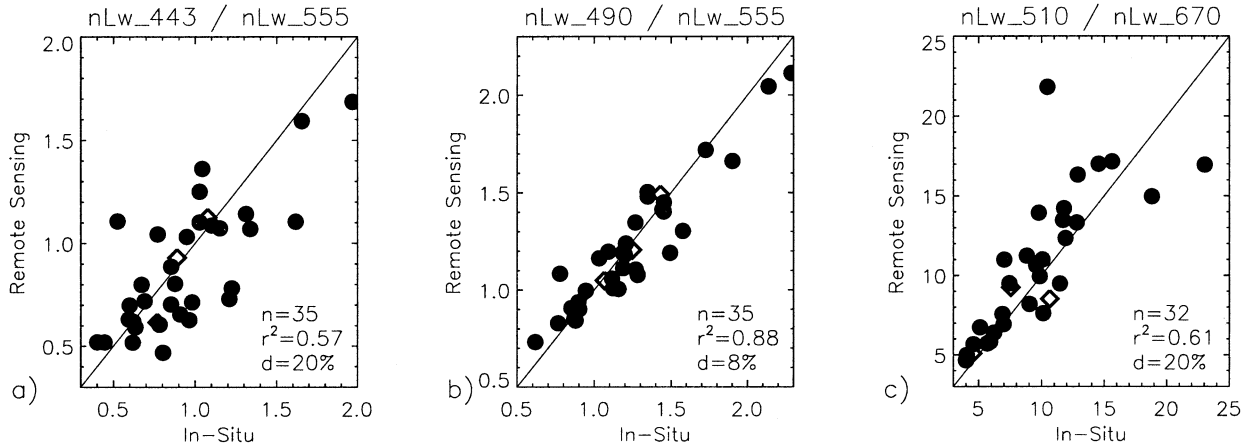

Fig. 6. Scatter plot of SeaWiFS-derived versus *in situ* value of the ratio of normalized water leaving radiances at (a) 490 and 555 nm, (b) 443 and 555 nm, and (c) 510 and 670 nm. The diamond symbols represent the matchups used for the determination of the vicarious calibration coefficients.

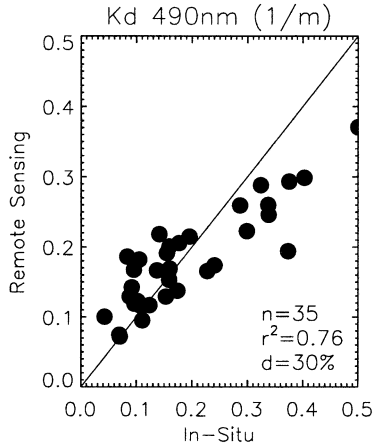

Fig. 7. Scatter plot of SeaWiFS-derived versus *in situ* K_d at 490 nm.

is used for the calculation of TSM (see Section III)]. The comparison does not include cases where the value of the normalized water leaving radiance at 670 nm is close to null (the threshold applied is 0.02 mW $\text{cm}^{-2}\text{sr}^{-1}\mu\text{m}^{-1}$). Those match-ups are evident in Fig. 3 and likely result from an overcorrection for aerosol at that wavelength. These cases are easily identified and discarded, since the corresponding ratio between the reflectance at 510 and 670 nm is much outside the range of values used for the algorithm development (i.e., ranging from 3 to 20).

Fig. 7 shows K_d at 490 nm computed with the algorithm described in Section III versus the *in situ* value for an optically homogeneous surface layer. The determination coefficient r^2 is 0.76, and the mean relative difference d is 30%. An overestimate is evident at values lower than 0.2 m^{-1}, whereas there is an underestimate for higher values. The comparison is consistent with Fig. 6 that shows a slight underestimation of the high ratios $\text{nL}_w(490\text{ nm})/\text{nL}_w(555\text{ nm})$ in the range of 1.5 to 2, and a slight overestimation of the low ratios in the range of 0.5 to 1.

C. Optically Significant Constituents

Laboratory measurements of *Chla* and TSM are compared in Fig. 8 with the values computed from the remote sensing normalized water leaving radiances nL_w applying the algorithms described in Section III. For the sake of comparison, *Chla* concentrations calculated with the operational algorithm OC4v4 developed for global applications [43] are displayed too.

The determination coefficient r^2 for the two chlorophyll a algorithms is similar (0.71 for AD versus 0.69 for OC4v4), but the mean relative percentage difference d is lower for the regional AD algorithm (40% versus 61%). An underestimate of *Chla* calculated by the AD algorithm is evident in the upper range. Conversely, the OC4v4 algorithm displays an overestimate of the concentration, more pronounced for the lower values. This algorithm takes as input the maximum of the three band ratios of the reflectance at 443–510 nm and the value at 555 nm. For the present dataset, most of the calculations leading to *Chla* concentrations lower (higher) than 1 mg m^{-3} were performed with the ratio between reflectances at 490 nm (510 nm) and 555 nm. Only two calculations used the reflectance at 443 nm. The overestimate of the low chlorophyll concentrations is therefore mostly traced to values of the ratio of R_{rs} at 490 and 555 nm.

The comparison for TSM concentration gives a determination coefficient r^2 of 0.75 and a mean relative percentage difference d of 28% for 32 match-ups. As for the comparison of band ratios, match-ups with a normalized water leaving radiance nL_w at 670 nm lower than 0.02 mW $\text{cm}^{-2}\text{sr}^{-1}\mu\text{m}^{-1}$ are not included in the analysis. In fact, the value of the satellite-derived normalized water leaving radiance can be very low in the red and subject to a high relative uncertainty. It is finally reported that the improvement due to the use of a turbid-water correction is noticeable (not shown), with a decrease in the mean relative difference of 7% compared to cases without correction.

To give sensitivity to the former results, *Chla* and TSM have been computed applying the remote sensing algorithms to the *in situ*, instead of remote sensing, normalized water leaving radiances. Results show an improvement of 0.04 in the determination coefficient for both *Chla* algorithms (i.e., AD and OC4v4) and a decrease in the mean relative percentage difference d of 8% (AD) and of 12% (OC4v4) (i.e., displaying mean relative percentage differences of 32% and 49%, respectively). For TSM, the mean relative percentage difference d shows a decrease from 28% to 22%. It is noticed that the results

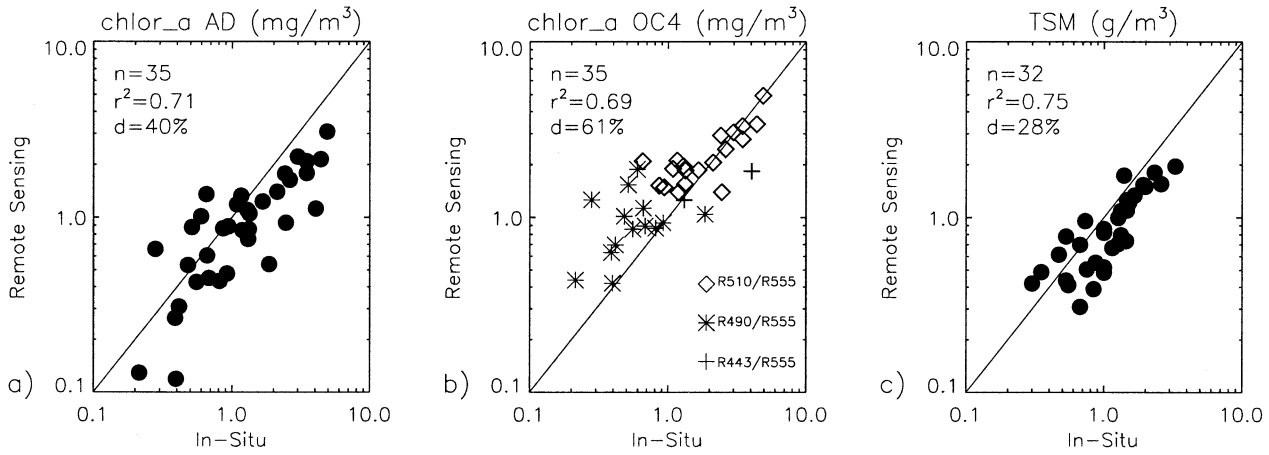

Fig. 8. Scatter plot of SeaWiFS-derived versus *in situ* optically active water constituents. (a) *Chla* computed with the AD algorithm, (b) *Chla* computed with the OC4v4 algorithm (the three symbols refer to the remote sensing reflectance ratio used as input to the algorithm), and (c) TSM.

obtained for the match-ups with the AD chlorophyll algorithm used with the *in situ* or remote sensing nL_w display similar trends (see Fig. 8 for remote sensing data), and specifically an underestimate of the higher concentrations. This result suggests that situations of relatively high reflectance ratios for the range of high *Chla* concentrations (greater than 1 mg m^{-3}) were overrepresented in the validation dataset with respect to the development dataset.

V. Conclusion

The validation of SeaWiFS primary products with *in situ* data collected at the AAOT site in the northern Adriatic has been carried out through the analysis of match-ups covering the period September 1997 to September 2001. Making use of a simple atmospheric correction scheme, the results have shown determination coefficients above 0.8 and relative differences below 23% for the aerosol optical thickness at all wavelengths. A similar comparison has given determination coefficients of about 0.8 and relative differences of 20% to 30% for the water leaving radiance from 490–670 nm, relative differences of 8% for their ratio at 490 and 555 nm, and a determination coefficient of 0.76 and relative difference of 30% for K_d at 490 nm.

It is noticed that this close agreement is not translated into a corresponding accuracy in the retrieval of optically significant constituents. In fact, for *Chla* and TSM, comparisons of *in situ* data and remote sensing concentrations obtained with empirical algorithms have given determination coefficients of 0.71 and 0.75 and relative mean percentage differences of 40% and 28%, respectively. It is pointed out that the results presented, particularly for *Chla*, are affected by a slightly biased statistical representativity of the validation dataset with respect to the multiyear time series of measurements used for the algorithms development.

This validation study further confirms that most of the uncertainty in the remote sensing determination of *Chla* and TSM is due to the intrinsic high level of uncertainty of the empirical in-water algorithms. The latter is explained by the highly varying contributions of the different optically significant substances to the physical signal, and the variability of their respective specific optical properties. Improvements could be brought by the use of analytical models and inversion techniques. However, the accuracy of the satellite-derived concentrations of optically significant constituents, calculated with simple band ratios empirical algorithms, may still be satisfactory for particular environmental applications.

In addition to the former specific conclusions, this study has highlighted the importance of the so-called turbid-water correction that takes into account a potential optical contribution of the water in the NIR, also for the moderately turbid northern Adriatic coastal waters.

Finally, this work underlines the importance of long-term accurate field measurements, including comprehensive atmospheric and marine data to support the validation of satellite products.

Acknowledgment

The authors would like to thank the SeaWiFS Project (Code 970.2) and the Distributed Active Archive Center (Code 902) at the Goddard Space Flight Center for the production and distribution of these data, respectively.

References

[1] S. B. Hooker and W. S. Esaias, "An overview of the SeaWiFS mission," *EOS Trans. Amer. Geophys. Union*, vol. 74, pp. 241–246, 1993.

[2] F. P. Chavez, P. G. Strutton, G. E. Friederich, R. A. Feely, G. C. Feldman, D. G. Foley, and M. J. McPhaden, "Biological and chemical response of the Equatorial Pacific Ocean to the 1997–98 El Niño," *Science*, vol. 286, pp. 2126–2131, 1999.

[3] R. G. Murtugudde, S. R. Signorini, J. R. Christian, A. J. Busalacchi, C. R. McClain, and J. Picaut, "Ocean color variability of the tropical Indo-Pacific basin observed by SeaWiFS during 1997–1998," *J. Geophys. Res.*, vol. 104, pp. 18 351–18 366, 1999.

[4] S. R. Signorini, R. G. Murtugudde, C. R. McClain, J. R. Christian, J. Picaut, and A. J. Busalacchi, "Biological and physical signatures in the tropical and subtropical Atlantic," *J. Geophys. Res.*, vol. 104, pp. 18 367–18 382, 1999.

[5] A. Longhurst, "A major seasonal phytoplankton bloom in the Madagascar basin," *Deep-Sea Res.*, pt. I, vol. 48, pp. 2413–2422, 2001.

[6] R. B. Husar, D. M. Tratt, B. A. Schichtel, S. R. Falke, F. Li, D. Jaffe, S. Gassó, T. Gill, N. S. Laulainen, F. Lu, M. C. Reheis, Y. Chun, D. Westphal, B. N. Holben, C. Gueymard, I. McKendry, N. Kuring, G. C. Feldman, C. McClain, R. J. Frouin, J. Merrill, D. DuBois, F. Vignola, T. Murayama, S. Nickovic, W. E. Wilson, K. Sassen, N. Sugimoto, and W. C. Malm, "Asian dust events of April 1998," *J. Geophys. Res.*, vol. 106, pp. 18 317–18 330, 2001.

[7] C. Moulin, H. R. Gordon, V. F. Banzon, and R. H. Evans, "Assessment of Saharan dust absorption in the visible from SeaWiFS imagery," *J. Geophys. Res.*, vol. 106, pp. 18 239–18 249, 2001.

[8] S. B. Hooker and C. R. McClain, "The calibration and validation of SeaWiFS data," *Prog. Oceanogr.*, vol. 45, pp. 427–465, 2000.

[9] C. R. McClain, W. E. Esaias, W. Barnes, B. Guenther, D. Endres, S. B. Hooker, G. Mitchell, and R. Barnes, "Calibration and validation plan for SeaWiFS," NASA Goddard Space Flight Center, Greenbelt, MD, SeaWiFS Tech. Rep. NASA Tech. Memo. 104 566, vol. 3, 1992.

[10] G. Zibordi, J. F. Berthon, J. P. Doyle, S. Grossi, D. van der Linde, C. Targa, and L. Alberotanza, "Coastal Atmosphere and Sea Time Series (CoASTS): A long-term measurement program," NASA Goddard Space Flight Center, Greenbelt, MD, SeaWiFS Tech. Rep. NASA Tech. Memo. 206 892, vol. 19, 2002.

[11] J.-F. Berthon, G. Zibordi, J. P. Doyle, S. Grossi, D. van der Linde, and C. Targa, "Coastal Atmosphere and Sea Time Series (CoASTS): Data analysis," NASA Goddard Space Flight Center, Greenbelt, MD, SeaWiFS Tech. Rep. NASA Tech. Memo. 206892, vol. 20, 2002.

[12] H. Loisel and A. Morel, "Light scattering and chlorophyll concentration in case 1 waters: A reexamination," *Limnol. Oceanogr.*, vol. 43, pp. 847–858, 1998.

[13] S. B. Hooker, G. Zibordi, G. Lazin, and S. McLean, "The SeaBOARR-98 field campaign," NASA Goddard Space Flight Center, Greenbelt, MD, SeaWiFS Tech. Rep. NASA Tech. Memo. 206 892, vol. 3, 1999.

[14] H. R. Gordon and D. K. Clark, "Clear water radiances for atmospheric correction of coastal zone color scanner," *Appl. Opt.*, vol. 20, pp. 4715–4180, 1981.

[15] B. N. Holben, T. F. Eck, I. Slutsker, D. Tanré, J. P. Buis, A. Stezer, E. Vermote, J. A. Reagan, Y. Kaufman, T. Nakajima, F. Lavenu, I. Jankowiak, and A. Smirnov, "AERONET—A federated instrument network and data archive for aerosol characterization," *Remote Sens. Environ.*, vol. 66, pp. 1–16, 1998.

[16] H. R. Gordon and K. Ding, "Self-shading of in-water optical instruments," *Limnol. Oceanogr.*, vol. 37, pp. 491–500, 1992.

[17] G. Zibordi and G. M. Ferrari, "Instrument self-shading in underwater optical measurements: Experimental data," *Appl. Opt.*, vol. 34, pp. 2750–2754, 1995.

[18] J. P. Doyle and G. Zibordi, "Monte Carlo modeling of optical transmission within 3-D shadowed field: Application to large deployment structures," *Appl. Opt.*, vol. 41, pp. 4283–4306, 2002.

[19] H. Neckel and D. Labs, "The solar radiation between 3300 and 12 500 Å," *Sol. Phys.*, vol. 90, pp. 205–258, 1984.

[20] C. Targa, D. van der Linde, and J.-F. Berthon, "The first SeaWiFS HPLC analysis round-robin experiment (SeaHARRE-1)—The JRC method," NASA Goddard Space Flight Center, Greenbelt, MD, SeaWiFS Tech. Rep. NASA Tech. Memo. 206 892, vol. 14, 2000.

[21] J. D. H. Strickland and T. R. Parsons, *A Practical Handbook of Seawater Analysis*, 2nd ed: Fisheries Research Board of Canada, 1972, vol. 167, pp. 181–184.

[22] T. F. Eck, B. N. Holben, J. S. Reid, O. Dubovik, A. Smirnov, N. T. O'Neill, I. Slutsker, and S. Kinne, "The wavelength dependence of the optical depth of biomass burning, urban and desert dust aerosols," *J. Geophys. Res.*, vol. 104, pp. 31 333–31 350, 1999.

[23] G. Zibordi and J.-F. Berthon, "Relationships between Q-factor and seawater optical properties in a coastal region," *Limnol. Oceanogr.*, vol. 46, pp. 1130–1140, 2001.

[24] S. B. Hooker, G. Zibordi, J.-F. Berthon, D. D'Alimonte, S. Maritorena, S. McClean, and J. Sildam, "Results of the second SeaWiFS data analysis round-robin, March 2000 (DARR-2000)," NASA Goddard Space Flight Center, Greenbelt, MD, SeaWiFS Tech. Rep. NASA Tech. Memo. 206 892, vol. 15, 2001.

[25] J. L. Mueller and R. W. Austin, "Ocean optics protocols for SeaWiFS validation," NASA Goddard Space Flight Center, Greenbelt, MD, SeaWiFS Tech. Rep. NASA Tech. Memo. 104 566, vol. 5, 1992.

[26] S. B. Hooker, H. Claustre, J. Ras, L. Van Heukelem, J.-F. Berthon, C. Targa, D. van der Linde, R. Barlow, and H. Sessions, "The first SeaWiFS HPLC Analysis Round-Robin Experiment (SeaHARRE-1)," NASA Goddard Space Flight Center, Greenbelt, MD, SeaWiFS Tech. Rep. NASA Tech. Memo. 206 892, vol. 14, 2000.

[27] R. A. Barnes, R. E. Eplee, Jr., S. F. Biggar, K. J. Thome, E. F. Zalewski, P. N. Slater, and A. W. Holmes, "The SeaWiFS solar radiation-based calibration and the transfer-to-orbit experiment," NASA Goddard Space Flight Center, Greenbelt, MD, SeaWiFS Tech. Rep. NASA Tech. Memo. 206 892, vol. 5, 1999.

[28] R. A. Barnes, R. E. Eplee, Jr., F. S. Patt, and C. R. McClain, "Changes in the radiometric sensitivity of SeaWiFS determined from lunar and solar-based measurements," *Appl. Opt.*, vol. 38, pp. 4649–4664, 1999.

[29] R. H. Evans and H. R. Gordon, "Coastal zone color scanner 'system calibration': A retrospective examination," *J. Geophys. Res.*, vol. 99, pp. 7293–7307, 1994.

[30] R. E. Eplee, Jr., W. D. Robinson, S. W. Bailey, D. K. Clark, P. J. Werdell, M. Wang, R. A. Barnes, and C. R. McClain, "Calibration of SeaWiFS. II. Vicarious techniques," *Appl. Opt.*, vol. 40, pp. 6701–6718, 2001.

[31] B. Sturm and G. Zibordi, "SeaWiFS atmospheric correction by an approximate model and vicarious calibration," *Int. J. Remote Sens.*, vol. 23, pp. 489–501, 2002.

[32] M. Wang, B. A. Franz, R. A. Barnes, and C. R. McClain, "Effects of the SeaWiFS band-pass on the retrieved ocean near-surface optical properties," *Appl. Opt.*, vol. 40, pp. 343–348, 2001.

[33] G. Fu, K. S. Baith, and C. R. McClain, "SeaDAS: The SeaWiFS Data Analysis System," in *Proc. 4th Pacific Ocean Remote Sensing Conf.*, Qingdao, China, 1998, pp. 73–79.

[34] M. Wang, "The SeaWiFS atmospheric correction algorithm updates," NASA Goddard Space Flight Center, Greenbelt, MD, SeaWiFS Tech. Rep. NASA Tech. Memo. 206 892, vol. 9, 2000.

[35] R. A. Arnone, P. Martinolich, R. W. Gould, R. Stumpf, and S. Ladner, "Coastal optical properties using SeaWiFS," in *Proc. Ocean Optics XIV*, Kailua-Kona, HI, 1998.

[36] H. R. Gordon, O. B. Brown, R. H. Evans, J. W. Brown, R. C. Smith, K. S. Baker, and D. K. Clark, "A semianalytic radiance model of ocean color," *J. Geophys. Res.*, vol. 93, pp. 10 909–10 924, 1988.

[37] A. Bricaud, M. Babin, A. Morel, and H. Claustre, "Variability in the chlorophyll-specific absorption coefficients of natural phytoplankton: Analysis and parameterization," *J. Geophys. Res.*, vol. 100, pp. 13 321–13 332, 1995.

[38] R. C. Smith and K. S. Baker, "Optical properties of the clearest natural waters," *Appl. Opt.*, vol. 20, pp. 177–184, 1981.

[39] G. M. Hale and M. R. Querry, "Optical constants of water in the 200-nm to 200-μm wavelength region," *Appl. Opt.*, vol. 12, pp. 555–563, 1973.

[40] H. Buiteveld, J. H. M. Hakvoort, and M. Donze, "The optical properties of pure water," in *Proc. Ocean Optics XII*, vol. 2258, J. S. Jaffe, Ed., 1994, pp. 174–183.

[41] D. A. Siegel, M. Wang, S. Maritorena, and W. D. Robinson, "Atmospheric correction of satellite ocean color imagery: The black pixel assumption," *Appl. Opt.*, vol. 39, pp. 3582–3591, 2000.

[42] A. Morel, "Optical modeling of the upper ocean in relation to its biogenous matter content (case 1 waters)," *J. Geophys. Res.*, vol. 93, pp. 10 749–10 768, 1988.

[43] J. E. O'Reilly, S. Maritorena, D. A. Siegel, M. C. O'Brien, D. Toole, B. G. Mitchell, M. Kahru, F. P. Chavez, P. Strutton, G. F. Cota, S. B. Hooker, C. R. McClain, K. L. Carder, F. Müller-Karger, L. Harding, A. Magnuson, D. Phinney, G. F. Moore, J. Aiken, K. R. Arrigo, R. Letelier, and M. Culver, "Ocean color chlorophyll a algorithms for SeaWiFS, OC2, OC4: Version 4," NASA Goddard Space Flight Center, Greenbelt, MD, SeaWiFS Tech. Rep. NASA Tech. Memo. 206 892, vol. 11, 2000.

[44] J. L. Mueller, "SeaWiFS algorithm for the diffuse attenuation coefficient, $K(490)$ using water-leaving radiances at 490 and 555 nm," NASA Goddard Space Flight Center, Greenbelt, MD, SeaWiFS Tech. Rep. NASA Tech. Memo. 2000-206 892, vol. 11, 2000.

[45] W. D. Robinson, G. M. Schmidt, C. R. McClain, and P. J. Werdell, "Changes made in the operational SeaWiFS processing," NASA Goddard Space Flight Center, Greenbelt, MD, SeaWiFS Tech. Rep. NASA Tech. Memo. 206 892, vol. 10, 2000.

[46] S. Bailey and M. Wang, "Satellite aerosol optical thickness match-up procedures," in *In situ aerosol optical thickness collected by the SIMBIOS program (1997–2000): Protocols, and data QC and analysis*. Greenbelt, MD: NASA Goddard Space Flight Center, 2001, pp. 70–72.

[47] A. Ångström, "Techniques of determining the turbidity of the atmosphere," *Tellus*, vol. 13, pp. 214–223, 1961.

[48] B. N. Holben, D. Tanré, A. Smirnov, T. F. Eck, I. Slutsker, N. Abuhassan, W. W. Newcomb, J. S. Schafer, B. Chatenet, F. Lavenu, Y. J. Kaufman, J. Vande Castle, A. Setzer, B. Markham, D. Clark, R. Frouin, R. Halthore, A. Karneli, N. T. O'Neill, C. Pietras, R. T. Pinker, K. Voss, and G. Zibordi, "An emerging ground-based aerosol climatology: Aerosol optical depth from AERONET," *J. Geophys. Res.*, vol. 106, pp. 12 067–12 097, 2001.

[49] J. E. O'Reilly, S. Maritorena, B. G. Mitchell, D. A. Siegel, K. L. Carder, S. A. Garver, M. Kahru, and C. R. McClain, "Ocean color chlorophyll algorithms for SeaWiFS," *J. Geophys. Res.*, vol. 103, pp. 24 937–24 953, 1998.

[50] M. Kahru and B. G. Mitchell, "Empirical algorithm and preliminary SeaWiFS validation for the California current," *Int. J. Remote Sens.*, vol. 20, pp. 3423–3429, 1999.

[51] J. L. Mueller and C. C. Trees, "Revised SeaWiFS prelaunch algorithm for the diffuse attenuation coefficient $K(490)$," NASA Goddard Space Flight Center, Greenbelt, MD, SeaWiFS Tech. Rep. NASA Tech. Memo. 104566, vol. 41, 1997.

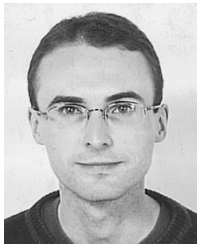

Frédéric Mélin received the diplôme d'ingénieur from the Ecole Nationale Supérieure de l'Aéronautique et de l'Espace, Toulouse, France, in 1995.

He was a Research Assistant from 1995 to 1997 at the Jet Propulsion Laboratory, California Institute of Technology, Pasadena, where he studied the seasonal to interannual variability of the equatorial Pacific and Indian oceans using ocean surface circulation models and satellite data. Since 1998, he has been working at the Joint Research Centre of the European Commission, Ispra, Italy, where his research focuses on the determination of atmospheric and marine optical properties based on optical remote sensing, and their application to the calculation of marine primary production. His main research interest is the use of satellite data and particularly ocean color, together with models, for the study of the marine biogeochemical cycles.

Giuseppe Zibordi received the Laurea degree in physics from the University of Modena, Modena, Italy, in 1981.

He was a Researcher at the Italian National Research Council, Modena, Italy, from 1984 to 1992, where he was involved in quantitative remote sensing of coastal and polar regions. Since 1993, he is with the Joint Research Centre of the European Commission, Ispra, Italy, involved in ocean color development and validation activities. His research interests include remote sensing methodologies for the determination of atmospheric and marine optical properties, and the absolute radiometric calibration of optical instruments.

Jean-François Berthon received the Ph.D. degree in biological oceanography from the Université "Pierre et Marie Curie," Paris, France.

He worked at the Joint Research Centre of the European Commission, Ispra, Italy, from 1995 to 2001, and is currently with the Maison de la Recherche en Environnement Naturel, Université du Littoral Côte D'Opale, Wimereux, France. His particular interests are marine bio-optical measurements and modeling, and application of ocean color remote sensing to marine primary production.